Chain dimensions and intermolecular interactions of polysilanes bearing alkyl side groups over the UV thermochromic temperature

XinYue Jiang[a], Ken Terao[a,*], Woojung Chung[b], Masanobu Naito[b,c,**]

[a] *Department of Macromolecular Science, Osaka University, 1-1, Machikaneyama-cho, Toyonaka, Osaka, 560-0043, Japan*

[b] *Graduate School of Materials Science, Nara Institute of Science and Technology, 8916-5 Takayama, Ikoma, Nara 630-0192 Japan*

[c] *National Institute for Materials Science (NIMS), 1-1 Namiki, Tsukuba, Ibaraki 305-0044, Japan*

* Corresponding author. Tel.: +81 6 6850 5459; fax: +81 6 6850 5461.

** Corresponding author. Tel.: +81 29 860 4783.

E-mail addresses: kterao@chem.sci.osaka-u.ac.jp (K. Terao), masanobu@nims.go.jp (M. Naito)

ABSTRACT

To elucidate temperature change of intermolecular interactions and chain dimensions for poly(dialkylsilane)s with or without thermochromism, synchrotron-radiation small-angle X-ray scattering and UV-absorption measurements were carried out for relatively low-molar mass poly(*n*-hexylmethyl)silane (**PSi-1**), poly(*n*-decylmethyl)silane (**PSi-2**), and poly(*n*-hexylpropyl)silane (**PSi-3**) samples in isooctane over a wide temperature range down to −94 °C. While the dimensional properties for the three polysilanes were almost irrespective of temperature, the second virial coefficient for **PSi-2** and **PSi-3** significantly decreased and became negative below the thermochromic temperature at −60 °C and −50 °C, respectively. Analyses in terms of the quasi-two-parameter theory for the wormlike chain showed that conformational change detected by UV-absorption behavior does not cause appreciably the unperturbed chain dimensions of the polysilane samples. Furthermore, aggregates were detected by ultra-small-angle X-ray scattering measurements for high molar mass **PSi-3** samples at low temperatures. These results indicate that intermolecular interactions between poly(dialkylsilane) molecules become attractive around the thermochromic temperature.

Key Words: polysilane; SAXS; intermolecular interaction

1. Introduction

Polymer dimensions in solution are one of the most important properties of macromolecules since it is well related to the physical properties of polymer solutions including viscoelasticity as well as lyotropic liquid crystallinity [1, 2]. Chain dimensions for stiff polymers including relatively short flexible polymers are mainly determined by the chain stiffness in the Kratky-Porod wormlike chain [3] while the intramolecular excluded-volume effects become more important for long flexible chains [4-6]. Polysilanes with Si-Si σ-bonded main chain have unique UV absorption band between 300 and 350 nm in wavelength [7, 8]. Thus, it can be used as light induced degradable segment of amphiphilic polymer micelles [9, 10] to obtain hollow particles [11, 12]. This conjugation length appreciably depends on the internal rotation of Si-Si backbone. From dimensional and hydrodynamic properties for poly(dialkylsilane)s in solution [13-23], significant correlation was found between the chain dimensions and UV absorption (and/or circular dichroism) [18, 24-26]. We also recently showed that the chain stiffness increases with sharpening the UV absorption band [27] and it is useful to discuss the wrapping behavior of carbon nanotubes [28].

Meanwhile, Harrah et al. [29] and Trefonas et al. [30] firstly found that some poly(dialkylsilane)s have significant UV thermochromism even in solution at low temperatures and numerous experimental and theoretical studies have been reported [31-37]. Since this temperature change of the main chain conformation should be caused by temperature dependent interactions between side alkyl groups, chain dimensions and intermolecular interactions might be different below and above the transition temperature. Miller, Shukla, and their coworkers [14, 38] found that chain dimensions for some poly(dialkylsilane)s with the weight-average molar mass M_w of ~10^6 g mol^{-1} are irrespective of temperature but significant aggregates were observed at or below the transition region by light and neutron scattering measurements, suggesting attractive intermolecular interactions

at low temperatures. However, the unperturbed dimensional properties near the thermochromic temperature is still unclear because they are significantly affected by the temperature change of the intramolecular excluded-volume effects. Contribution from this effect can be estimated in terms of the current theories [4] for perturbed wormlike chains if the chain length is not very long since the excluded volume effect diminishes and the solubility generally becomes better with lowering M_w. Furthermore, there is a need to ascertain whether recently reported relationship between the UV absorption spectra and the chain stiffness [27] is applicable at and below the thermochromic temperature.

We thus made small-angle X-ray scattering measurements in solution at various temperatures for three polysilanes having relatively low M_w, that is, poly(*n*-hexylmethyl)silane (**PSi-1**), poly(*n*-decylmethyl)silane (**PSi-2**), and poly(*n*-hexylpropyl)silane (**PSi-3**) of which chemical structures are shown in Fig. 1. Both **PSi-2** and **PSi-3** have UV thermochromism in THF at −60 °C and −40 °C, respectively, while UV-absorption peak for **PSi-1** only gradually red-shifts and slightly sharpens with lowering temperature. In this study, we chose isooctane as a solvent in which the polysilanes samples have much higher X-ray contrast than those in THF. In our preliminary experiment, we have checked that similar temperature induced peak shifts in the UV spectra were found in isooctane. The obtained temperature dependent polymer dimensions and intermolecular interactions were compared with the UV spectra at each temperature.

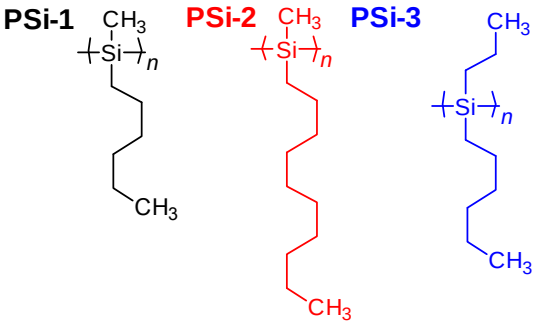

Fig. 1. Chemical structures of poly(*n*-hexylmethyl)silane (**PSi-1**), poly(*n*-decylmethyl)silane (**PSi-2**), and poly(*n*-hexylpropyl)silane (**PSi-3**).

2. Experimental section

2.1. Samples and solvents

The sodium-mediated Wultz coupling method [7, 8, 26] in refluxed toluene was utilized to synthesize **PSi-1**, **PSi-2**, and **PSi-3** samples. Fractional precipitation procedures were performed for the obtained samples with three precipitants, methanol, ethanol, and isopropanol, to reduce the molar mass dispersity. We chose a **PSi-1** sample, a **PSi-2** sample, and three **PSi-3** samples for this study and designated them as PSi-1-31k, PSi-2-64k, PSi-3-84k, PSi-3-210k, and PSi-3-1200k of which numbers from 31 to 1200 indicate the weight average molar masses M_w in unit of 10^3g mol^{-1}. The number-average molar mass M_n and M_w were estimated from the size exclusion chromatography (SEC) in THF equipped with refractive index and viscosity detectors in terms of the universal calibration method [39-41] as is the case with our recent study [27]. The obtained dispersity indices (M_w/M_n) for PSi-1-31k, PSi-2-64k, PSi-3-84k, PSi-3-210k, and PSi-3-1200k were determined to be 1.3, 1.2, 1.2, 1.5, and 1.5, respectively. Isooctane distilled over calcium hydride was used as a solvent for the following measurements.

2.2. UV-spectroscopy

UV absorption spectra for PSi-1-31k, PSi-2-64k, and PSi-3-84k in isooctane from −100 °C to 25 °C were evaluated by using a JASCO V-550 spectrophotometer with a UNISOKU CoolSpeK USP-203-CD-B cryostat. Molar concentration of repeat unit c_m was set to be from 4×10^{-5} mol L^{-1} to 0.1 mol L^{-1}. A rectangular quartz cell with the path length of 10 mm and a demountable quartz cell with the path length of 0.01 mm were used to adjust the absorbance at the peak to be between 0.2 and 2.

2.3. Small-angle X-ray scattering (SAXS)

Small-angle X-ray scattering measurements were made for three relatively low M_w samples, PSi-1-31k, PSi-2-64k, and PSi-3-84k in isooctane at various temperatures from −94 °C to 90 °C at the BL40B2 beamline in SPring-8. Scattering intensity was evaluated as a function of the magnitude of scattering vector q from the circular average method. Two dimensional scattering intensity data were recorded by a RIGAKU R-AXIS VII imaging plate. The obtained scattering intensity $I(q)$ was normalized by the intensity of the incident light and transmittance of the X-ray by means of the ionization chambers installed at the upper and lower side of the cell. The camera length, accumulation time, and wavelength were chosen to be 1.5 – 4 m, 90 – 180 sec, and 0.10 nm, respectively. The actual camera length was determined by means of the Bragg reflection of silver behenate. Solvent and four solutions having different polymer mass concentration c were measured in a specially designed 2 mmϕ capillary cell [42] at low temperatures up to 25 °C and a conventional 2 mmϕ capillary cell at higher temperatures. Solvent and solution temperatures were thermostated by means of an OXFORD Cryojet nitrogen jet with the flow rate of 8000 cm^3min^{-1} and a shield flow of 6000 cm^3min^{-1} for the former cell and the INSTEC HCS-302 system for the latter. The

excess scattering intensity $\Delta I(q)$ at each q was determined as a difference in $I(q)$ between solution and solvent in the same capillary cell.

Ultra-small-angle X-ray scattering (USAXS) measurements were performed for the two high M_w samples, PSi-3-210k and PSi-3-1200k in isooctane in the temperature range from −76 °C to 25 °C at the BL19B2 beamline in SPring-8 [43]. The wavelength, the camera length, and the accumulation time were set to be 0.069 nm, 40 m, and 1200 sec, respectively. Scattered light were detected by a DECTRIS PILATUS-2M hybrid pixel detector. The Bragg reflection of collagen were used to determine actual camera length. The intensity of direct X-ray and transmittance were determined by the same detector without the beam stopper (3 mmϕ). The same cell and cryojet were used as those for the former SAXS measurements. Test solutions with three different concentrations ranging from 4×10^{-3} g cm^{-3} to 1×10^{-2} g cm^{-3} were prepared for each sample to determine $\Delta I(q) / c$ at zero concentration as is the case with the SAXS measurements. Because the scattering intensity from air was not enough weak, meaningful values for $\Delta I(q)$ were only evaluated at the two lowest temperatures, −76 °C and −67 °C.

3. Results and discussion

3.1. Temperature induced conformational change in isooctane as deduced from UV spectroscopy.

Local conformational change of the main chain of polysilanes reflects the absorption spectra of near ultraviolet region as described in Introduction. As some examples, UV-absorption spectra between 250 nm and 400 nm are displayed in Fig. 2. As is the case with our recent research in THF [27], the peak shapes both for **PSi-2** and **PSi-3** drastically change in the intermediate temperature range whereas that for **PSi-1** monotonically shifts. It should be noted that an isosbestic point is found for **PSi-2** in isooctane below −60 °C. Similar

behavior were reported for THF solution in our previous paper [27] and other poly(dialkylsilane)s suggesting two different conformations of the Si-Si backbone. The obtained wavelength λ_{max} and the molar extinction coefficient of the repeat unit ε_{max} at the peak are plotted against temperature T in Fig. 3. While both λ_{max} and ε_{max} for **PSi-1** gradually increase with lowering temperature, the values of λ_{max} for **PSi-2** and **PSi-3** abruptly increase about −60 °C and −40 °C, respectively. On the contrary, ε_{max} for **PSi-2** has a slight minimum at the transition temperature, −60 °C, whereas temperature dependence of **PSi-3** has a rapid rise with lowering temperature around −50 °C. These trends are similar to those in THF as reported previously [27]. Filled symbols in the figure indicate the data points for solutions with high concentration which is substantially the same as those for SAXS measurements. They are fairly fitted by those for the low concentration data, indicating that intermolecular interactions between polymer chains do not significantly affect the main chain conformation. It should be noted that there are no ε_{max} data for high c_m solutions in the figure because of low reproducibility of polymer mass concentration in the thin demountable cell.

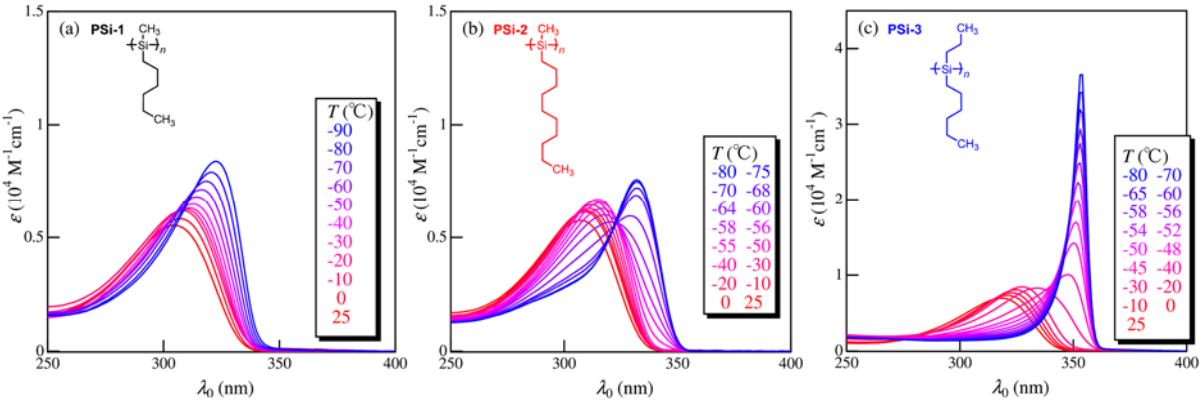

Fig. 2. UV-absorption spectra (the molar extinction coefficient ε of the monomer unit vs the wavelength λ_0 in vacuum) for PSi-1-31k (a), PSi-2-64k (b), and PSi-3-84k (c) in isooctane at indicated temperatures. Molar concentration of the repeat unit c_m was set to be 4×10^{-5} mol L^{-1}.

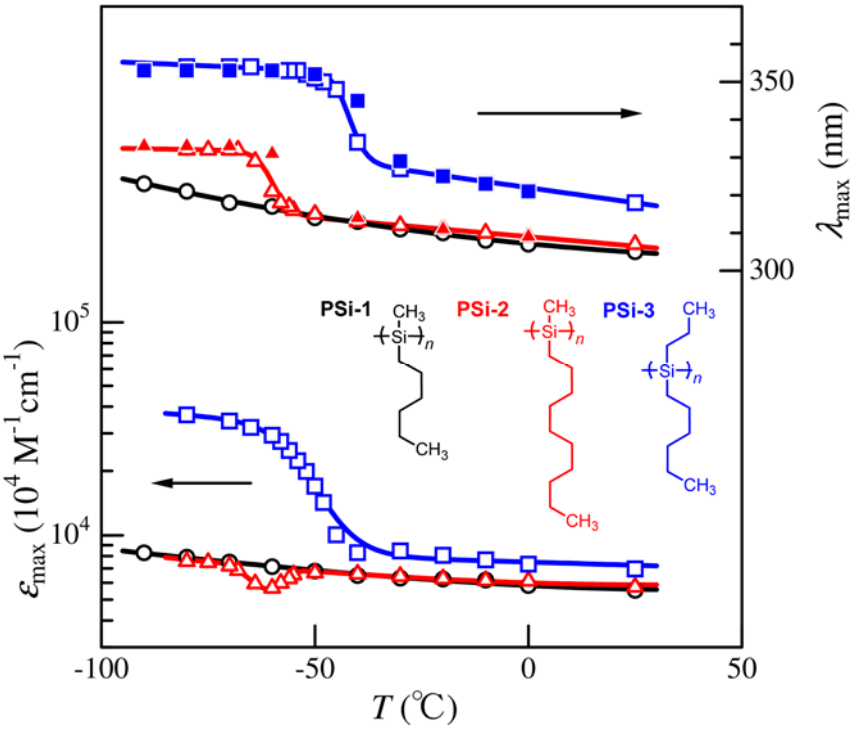

Fig. 3. Temperature dependence of λ_{max} and ε_{max} for PSi-1-31k (circles), PSi-2-64k (triangles), and PSi-3-84k (squares) in isooctane. Unfilled and filled symbols indicate $c_m = 4 \times 10^{-5}$ mol L^{-1} and 0.1 mol L^{-1}, respectively.

3.2. Scattering behavior of the polysilanes in isooctane over a wide temperature range.

Fig. 4 illustrates the Zimm plots [44] from SAXS measurements for PSi-3-84k in isooctane at −20 °C and −67 °C. While the Berry plot [45] should be more suitable to determine the *z*-average mean square radius of gyration $\langle S^2 \rangle_z$ for flexible and semiflexible polymers, we chose this plot because of the better linearity of the experimental data. This might be due to quite broad molar mass distribution, $M_w / M_n = 1.2 – 1.3$. The values for $c / \Delta I(q)$ at infinite dilution and at $q^2 = 0$ are similar at the two temperatures, and furthermore, the $[c/\Delta I(0)]_{c=0}$ data obtained for exactly the same capillary cell and sample were fairly close, suggesting that PSi-1-31k, PSi-2-64k, and PSi-3-84k molecularly disperse in isooctane at the temperature range investigated.

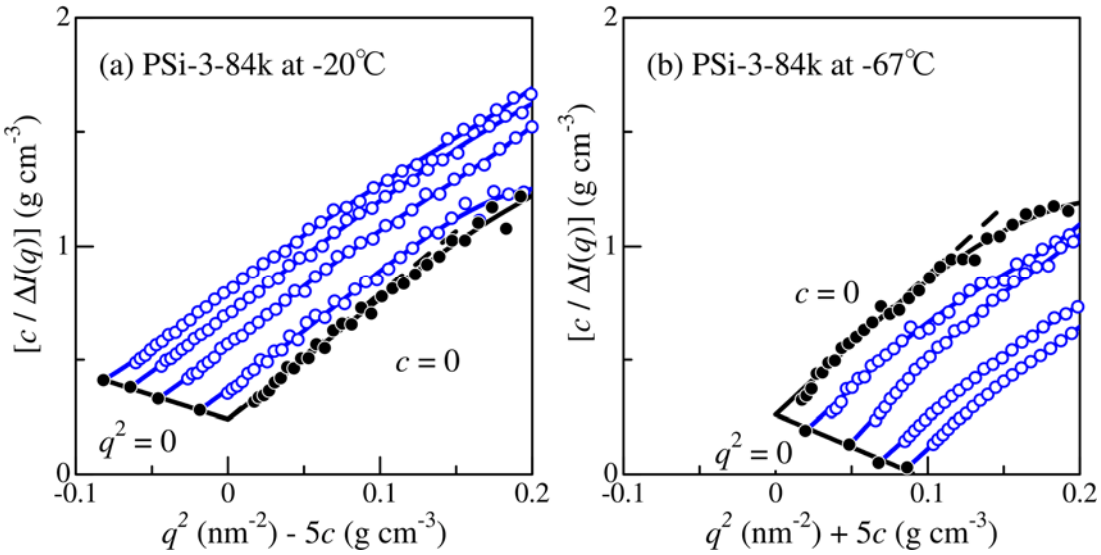

Fig. 4. Zimm plots for PSi-3-80k in isooctane at −20 °C (a) and −67 °C (b), respectively. Unfilled and filled circles indicate the experimental data and the extrapolated values to zero concentration or zero scattering vector, respectively. Broken lines denote the initial slope to determine $\langle S^2 \rangle_z$.

The obtained $\langle S^2 \rangle_z^{1/2}$ values for PSi-1-31k, PSi-2-64k, and PSi-3-84k are plotted against temperature in Fig. 5. The particle scattering functions at the higher q range were not further analyzed because of less repeatability. This is probably due to the less scattering intensity than those for our previously investigated polystyrene [42]. In the low temperature range including the thermochromic region, $\langle S^2 \rangle_z^{1/2}$ for PSi-2-64k and PSi-3-84k slightly increases with lowering temperature while those for PSi-1-31k almost independent of temperature, suggesting there are no significant change in the global conformation of the investigated polysilanes. Conversely, plots of $c/\Delta I(0)$ vs c at the two temperatures have opposite slopes as shown in Fig. 4. The second virial coefficient A_2 can be estimated from the slope $\partial[c/\Delta I(0)] / \partial c$ and the intercept $[c/\Delta I(0)]_{c=0}$ by

$$A_2 = \frac{\partial\left[c/\Delta I(0)\right]/\partial c}{2\left[c/\Delta I(0)\right]_{c=0} M_w} \quad (1)$$

where M_w evaluated from the SEC measurements with the universal calibration method (see Experimental section) was used. Fig. 6 plots the obtained A_2 data against temperature for the three polysilanes samples. **PSi-1** has positive A_2 at all temperatures investigated. The A_2 data for **PSi-2** and **PSi-3** are also almost independent of temperature above −50 °C but rapidly decrease with lowering temperature and negative A_2 are observed, suggesting both **PSi-2** and **PSi-3** in isooctane have theta temperatures, at which A_2 for polymer samples having sufficiently high molar mass vanishes. Interestingly, these theta temperatures seem to be close but somewhat lower than the thermochromic temperature shown in Fig. 3. The appreciably lower transition temperature of A_2 is likely because A_2 is caused not only by the interaction between alkyl side groups covering the polysilane main chain but also by the chain thickness of the polysilane while the latter effect should be negligible for the thermochromic behavior. Consequently, the temperature induced local conformational change is mainly caused by the interactions between the side chains, and furthermore this change also makes the intermolecular interactions between poly(dialkylsilane)s attractive while those for the global conformation do not appreciably change.

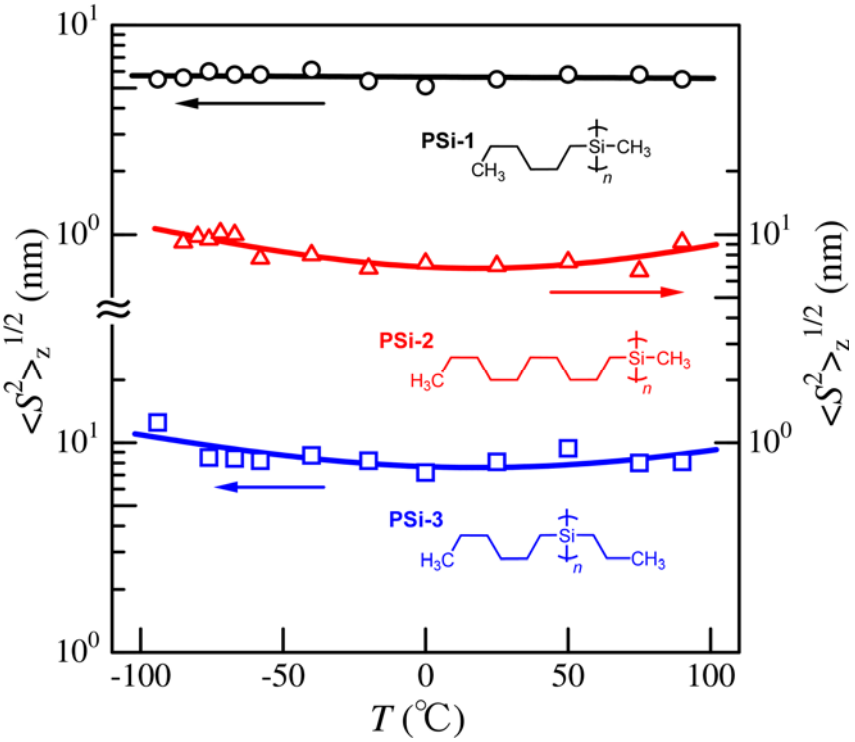

Fig. 5. Temperature dependence of the radius of gyration $\langle S^2 \rangle_z^{1/2}$ for PSi-1-31k (circles), PSi-2-64k (triangles), and PSi-3-84k (squares) in isooctane.

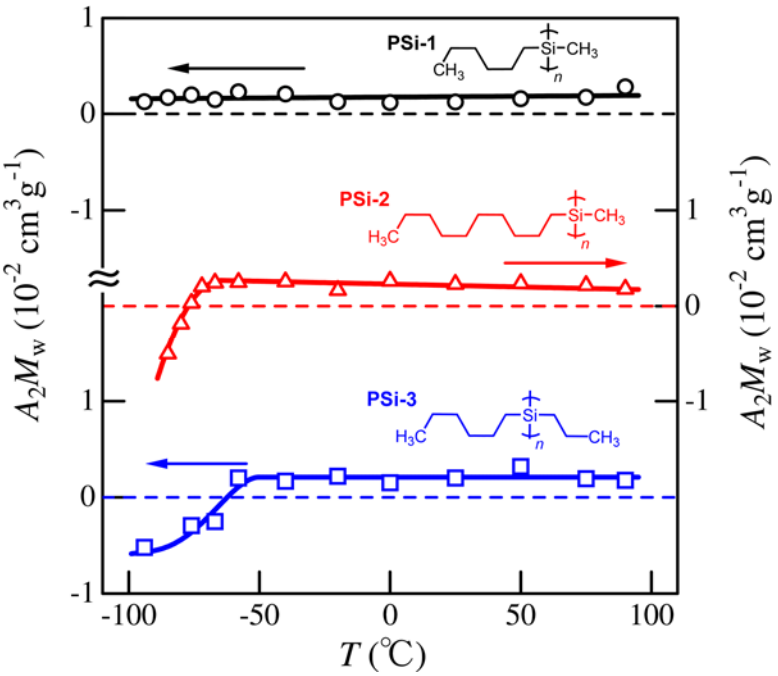

Fig. 6. Temperature dependence of the second virial coefficient A_2 for PSi-1-31k (circles), PSi-2-64k (triangles), and PSi-3-84k (squares) in isooctane.

3.3. Correlation among local conformation, chain dimensions, and intermolecular interactions.

According to our previous research for poly(dialkylsilane)s [27], molar extinction coefficient ε and the persistence length have a good correlation. If we now use the Kuhn segment length λ^{-1} for the chain stiffness, the relationship (eq 1 in ref [27]) can be written as

$$\lambda^{-1} = \left(2000\varepsilon_{\max}{}^{-1} - 0.0432\right)^{-0.813} \tag{2}$$

for poly(dialkylsilane)s at the temperatures from −27 °C to 45 °C. The λ^{-1} value calculated from eq 2 with the corresponding $\varepsilon_{\max}$ data reproduces the experimentally determined λ^{-1} within ± 40% (average accuracy is ± 20%) for $\lambda^{-1} < 20$ nm. The radius of gyration for the unperturbed wormlike chain $\langle S^2\rangle_0$ is related to λ^{-1} in terms of the Benoit-Doty equation [46] as

$$\left\langle S^2 \right\rangle_0 = \frac{L}{6\lambda} - \frac{1}{4\lambda^2} + \frac{1}{4\lambda^3 L} - \frac{1}{8\lambda^4 L^2}\left[1 - \exp\left(-2\lambda L\right)\right] \tag{3}$$

where the contour length L is proportional to the molar mass of the polymer by

$$L = \frac{M_w h}{M_0} \tag{4}$$

with h and M_0 being the contour length per residue and the molar mass of the monomer unit, respectively. The former parameter h for four poly(dialkylsilane)s are reported to be 0.20 nm [20-23]. If we assume this value for the current polysilanes, $\langle S^2\rangle_0$ can be calculated from ε without fitting parameters. The resultant $\langle S^2\rangle_0{}^{1/2}$ are plotted as dashed lines and small unfilled symbols against temperature along with the experimentally determined $\langle S^2\rangle_z{}^{1/2}$ in Fig. 7. Even at high temperatures, experimental $\langle S^2\rangle_z{}^{1/2}$ are at most 35% larger than the calculated

value. This is most likely due to the intramolecular excluded-volume effects as well as quite broad molar mass distribution. The radius of gyration $\langle S^2 \rangle$ taking the former effect into account may be written as

$$\left\langle S^2 \right\rangle = \alpha_s^2 \left\langle S^2 \right\rangle_0 \tag{5}$$

The gyration-radius expansion factor α_s may be given in the quasi-two-parameter (QTP) scheme [4, 47-49] by the Domb-Barrett equation [50],

$$\alpha_s^2 = \left[1 + 10\tilde{z} + \left(\frac{70\pi}{9} + \frac{10}{3} \right) \tilde{z}^2 + 8\pi^{3/2} \tilde{z}^3 \right]^{2/15} \left[0.933 + 0.067 \exp\left(-0.85\tilde{z} - 1.39\tilde{z}^2 \right) \right] \tag{6}$$

The intramolecular scaled excluded-volume parameter $\tilde{z}$ is related to the conventional excluded volume parameter z by

$$\tilde{z} = \frac{3}{4} K\left(\lambda L\right) z \tag{7}$$

with

$$z = \left(\frac{3}{2\pi} \right)^{2/3} \left(\lambda B\right) \left(\lambda L\right)^{1/2} \tag{8}$$

Here, $K(\lambda L)$ is a known increasing function of λL and the value for the current systems ranges in 0.16 and 0.90 for λL = 2.85 and 34.1, respectively. Consequently, unknown parameter is only the excluded-volume strength B.

In this study, the parameter B was estimated from A_2 in terms of the Yamakawa theory [4, 51]. When the chain end effects on A_2 is negligible, A_2 may be written with the Avogadro number N_A, and the molar mass M as

$$A_2 = \frac{N_A L^2 B}{2M^2}\left(1 + 7.74\hat{z} + 52.3\hat{z}^{27/10}\right)^{-10/27} \tag{9}$$

and

$$\hat{z} = \frac{Q(\lambda L)}{2.865\alpha_s^3} z \tag{10}$$

where $Q(\lambda L)$ is a known function of λL and ranges from 1.7 to 2.4 for the current λL values for our polysilanes samples. The excluded-volume strength B at 25 °C was estimated to be 1.0 nm, 3.4 nm, 0.74 nm for PSi-1-31k, PSi-2-64k, and PSi-3-84k, respectively. They were used to calculate $\langle S^2 \rangle$ while the B values were somewhat smaller or larger than those evaluated from the intrinsic viscosity [27]. Assuming eq 2 is applicable for all temperature range, $\langle S^2 \rangle$ may be calculated as a function of temperature only from experimentally determined ε_{max} and A_2 from eqs 3 – 10 except for negative A_2 range since the QTP theory is only valid for zero or positive z. It should be noted that A_2 at each temperature was estimated by using an interpolation method. The evaluated $\langle S^2 \rangle$ are plotted as solid curves with filled small symbols in Fig. 7. At the lowest temperature for PSi-2-64k and the two lowest temperatures for PSi-3-84k, $\langle S^2 \rangle$ are not calculated because of negative A_2. While the calculated $\langle S^2 \rangle$ are fairly close to the experimental data above the thermochromic temperature, the $\langle S^2 \rangle$ data from SAXS below the temperature are significantly larger (PSi-2-64k) or smaller (PSi-3-84k) than the calculated values. This indicates that the dimensional properties for the current poly(dialkylsilane)s cannot be determined only from the universal relationship between UV absorption and the chain stiffness constructed from the data above the thermochromic temperature. According to Sato et al. [24, 25], the chain stiffness determined from the global conformation reflects helix reversals from their investigation for poly(dialkylsilane)s bearing chiral side groups because the helix reversals may behave as

'kink'. However, it is infeasible to estimate frequency of helix reversals or the helix persistence length because the current polysilanes samples are achiral. Therefore, if optically active polysilanes having thermochromic behavior in solution were found, this discrepancy might be elucidated. In any case, if high ε_{max} for **PSi-3** at low temperatures indicates high chain stiffness, helix reversals (kinks) should increase with lowering temperature to take into account the temperature irrespective $<S^2>_z$. Thus, long rodlike part may not exist for the current polysilane chains in solution even below the thermochromic temperature.

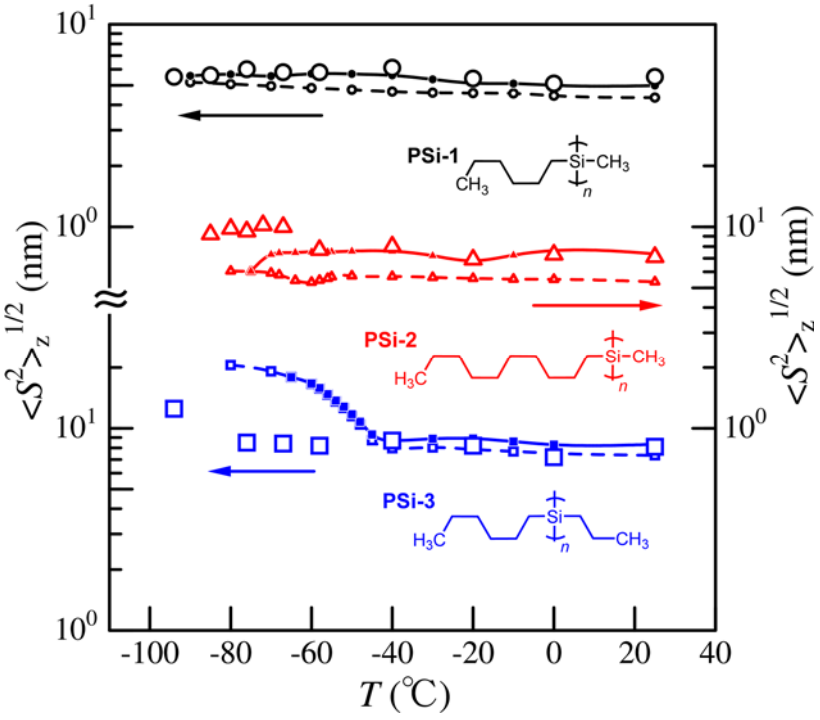

Fig. 7. Comparison between experimental (large circles) and calculated (small circles) radius of gyration for PSi-1-31k (circles), PSi-2-64k (triangles), and PSi-3-84k (squares). Small filled and unfilled circles denote the calculated values with or without the intramolecular excluded volume effects by means of the QTP theory.

3.3. Aggregation behavior of high molar mass PSi-3 samples.

According to the conventional Flory-Huggins theory [52], phase separation temperature for the polymer-solvent system having upper critical solution temperature significantly raises and approaches the theta temperature with increasing molar mass of the polymer. Thus, phase separation behavior or aggregation behavior may be observable for higher molar mass polysilane samples at low temperature. Since concentration dependence of the normalized scattering intensities $\Delta I(q)/c$ determined for PSi-3-210k and PSi-3-1200k are mostly independent of polymer mass concentration, the extrapolated values $[\Delta I(q)/c]_{c=0}$ to infinite dilution are plotted against q^2 in Fig. 8. Significant scattering intensity were only found at −67 °C and −76 °C. Those are below the theta temperature estimated for PSi-3-84k, clearly indicating the formation of aggregation. Similar behavior were found for the other high molar mass poly(dialkylsilane)s [14, 38]. Since the appropriate Guinier ranges are not available for the data, we compared the data with the particle scattering function of rigid spheres which is written as

$$P(q) = \left[\frac{3(\sin Rq - Rq\cos Rq)}{R^3 q^3} \right]^2 \tag{11}$$

While the theoretical values calculated by eq 11 have fluctuate even at high q range, log-normal distribution for the radius R of the sphere was applied to calculate the z-average particle scattering function $P_z(q)$. The solid curves are the calculated theoretical values of $P_z(q)$ for the median radius of the sphere are 500 – 600 nm and the ratios of weight-average to number-average radii were 1.5 – 2.0, suggesting submicron sized large number of aggregates exist in the PSi-3-210k and PSi-3-1200k solutions at low temperatures. This result strongly supports the temperature induced change of intermolecular interactions for the poly(dialkylsilane)s having thermochromic behavior.

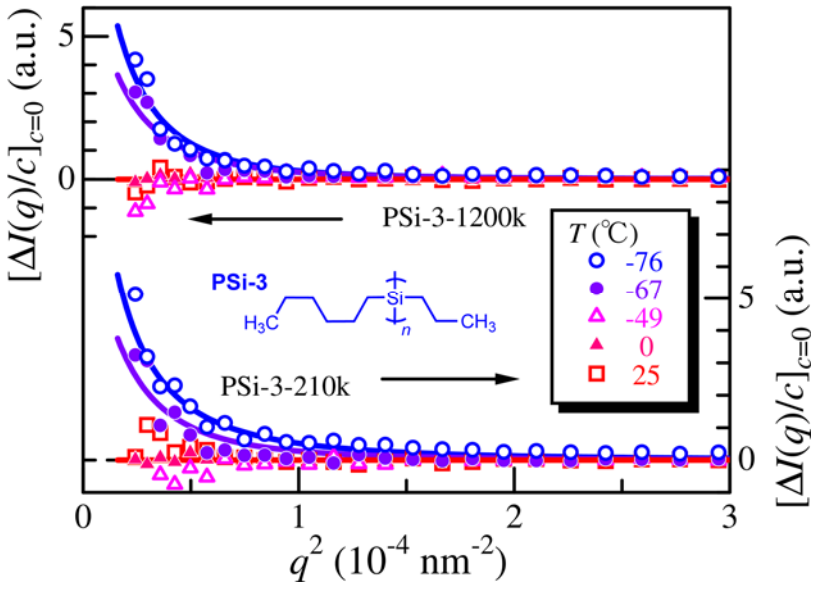

Fig. 8. Angular dependence of the excess scattering intensity $[\Delta I(q)/c]_{c=0}$ for PSi-3-1200k and PSi-3-210k in isooctane at −76 °C (unfilled circles), −67 °C (filled circles), −49 °C (unfilled triangles), 0 °C (filled triangles), and 25 °C (squares). Solid curves indicate the theoretical values for size-distributed spheres (see text).

4. Conclusions

We successfully determined radius of gyration for three low-molar mass poly(dialkylsilane)s with or without UV thermochromism in the investigated temperature range from −94 °C to 90 °C. The obtained chain dimensions are mostly irrespective of temperature and they are well explained by the previous relationship between the chain stiffness and the UV-absorption above the thermochromic temperature while appreciable difference was observed for **PSi-2** and **PSi-3** at lower temperatures, suggesting the limitation of the relationship. Furthermore, the coil to rod conformational transition induced by temperature were not observed in the dimensional properties even though we investigated low molar mass samples of which intramolecular attractive and/or repulsive interactions may not cause significantly the chain dimensions. Conversely, negative second virial coefficients

for low M_w **PSi-2** and **PSi-3** samples and aggregation behavior for high M_w **PSi-3** samples were observed at lower temperatures. It follows from these that intermolecular interactions may significantly change for other polysilanes having thermochromism in solution.

Acknowledgment

The authors thank Prof. Takahiro Sato in Osaka University for productive discussion, Dr. Masugu Sato and Dr. Noboru Ohta for their help in setting up the USAXS and SAXS apparatus in SPring-8. The synchrotron radiation experiments were performed at the BL40B2 and BL19B2 of SPring-8 with the approval of the Japan Synchrotron Radiation Research Institute (JASRI) (Proposal Nos. 2012A1059, 2012B1050, 2013A1046, and 2013B1515). This work was partially supported by JSPS KAKENHI Grant No. 25410130.

References

1. Sato T, Teramoto A. Adv Polym Sci 1996;126:85-161.
2. Sato T. Kobunshi Ronbunshu 2012;69:613-22.
3. Kratky O, Porod G. Recl Trav Chim Pays-Bas 1949;68:1106-22.
4. Yamakawa H. Helical Wormlike Chains in Polymer Solutions. Berlin, Germany: Springer, 1997.
5. Norisuye T. Prog Polym Sci 1993;18:543-84.
6. Norisuye T, Tsuboi A, Teramoto A. Polym J 1996;28:357-61.
7. West R. J Organomet Chem 1986;300:327-46.
8. Miller RD, Michl J. Chem Rev 1989;89:1359-410.
9. Sanji T, Nakatsuka Y, Kitayama F, Sakurai H. Chem Commun 1999:2201-02.

10. Sanji T, Kitayama F, Sakurai H. Macromolecules 1999;32:5718-20.

11. Sanji T, Nakatsuka Y, Ohnishi S, Sakurai H. Macromolecules 2000;33:8524-26.

12. Sakurai H. P Jpn Acad B-Phys 2006;82:257-69.

13. Cotts PM, Miller RD, Trefonas PT, West R, Fickes GN. Macromolecules 1987;20:1046-52.

14. Shukla P, Cotts PM, Miller RD, Russell TP, Smith BA, Wallraff GM, Baier M, Thiyagarajan P. Macromolecules 1991;24:5606-13.

15. Cotts PM, Ferline S, Dagli G, Pearson DS. Macromolecules 1991;24:6730-35.

16. Cotts PM. Macromolecules 1994;27:2899-903.

17. Cotts PM. J Polym Sci, Part B: Polym Phys 1994;32:771-78.

18. Fujiki M. J Am Chem Soc 1996;118:7424-25.

19. Kato H, Sasanuma Y, Kaito A, Tanigaki N, Tanabe Y, Kinugasa S. Macromolecules 2001;34:262-68.

20. Terao K, Terao Y, Teramoto A, Nakamura N, Terakawa I, Sato T. Macromolecules 2001;34:2682-85.

21. Terao K, Terao Y, Teramoto A, Nakamura N, Fujiki M, Sato T. Macromolecules 2001;34:4519-25.

22. Teramoto A, Terao K, Terao Y, Nakamura N, Sato T, Fujiki M. J Am Chem Soc 2001;123:12303-10.

23. Natsume T, Wu LB, Sato T, Terao K, Teramoto A, Fujiki M. Macromolecules 2001;34:7899-904.

24. Sato T, Terao K, Teramoto A, Fujiki M. Macromolecules 2002;35:2141-48.

25. Sato T, Terao K, Teramoto A, Fujiki M. Polymer 2003;44:5477-95.

26. Fujiki M, Koe JR, Terao K, Sato T, Teramoto A, Watanabe J. Polym J 2003;35:297-344.

27. Chung WJ, Shibaguchi H, Terao K, Fujiki M, Naito M. Macromolecules 2011;44:6568-73.

28. Chung W, Nobusawa K, Kamikubo H, Kataoka M, Fujiki M, Naito M. J Am Chem Soc 2013;135:2374-83.

29. Harrah LA, Zeigler JM. Journal of Polymer Science: Polymer Letters Edition 1985;23:209-11.

30. Trefonas P, Damewood JR, West R, Miller RD. Organometallics 1985;4:1318-19.

31. Schweizer KS. Synth Met 1989;28:C565-C72.

32. Klingensmith KA, Downing JW, Miller RD, Michl J. J Am Chem Soc 1986;108:7438-39.

33. Yuan CH, West R. Macromolecules 1994;27:629-30.

34. Sanji T, Sakamoto K, Sakurai H, Ono K. Macromolecules 1999;32:3788-94.

35. Kuzmany H, Rabolt JF, Farmer BL, Miller RD. J Chem Phys 1986;85:7413.

36. Bukalov SS, Leites LA, West R. Macromolecules 2001;34:6003-04.

37. Bande A, Michl J. Chemistry 2009;15:8504-17.

38. Miller RD, Wallraff GM, Baier M, Cotts PM, Shukla P, Russell TP, De Schryver FC, Declercq D. J Inorg Organomet Polym 1991;1:505-30.

39. Grubisic Z, Rempp P, Benoit H. J Polym Sci Pol Lett 1967;5:753-59.

40. Gu H, Nakamura Y, Sato T, Teramoto A, Green MM, Andreola C. Polymer 1999;40:849-56.

41. Farmer BS, Terao K, Mays JW. Int J Polym Anal Charact 2006;11:3-19.

42. Terao K, Morihana N, Ichikawa H. Polym J 2014;46:155-59.

43. Experimental procedure and preliminary experimental results are available at http://support.spring8.or.jp/Report_JSR/PDF_JSR_25B/2013B1515.pdf (in Japanese).

44. Zimm BH. J Chem Phys 1948;16:1099-116.

45. Berry GC. J Chem Phys 1966;44:4550-64.

46. Benoit H, Doty P. J Phys Chem 1953;57:958-63.

47. Yamakawa H, Stockmayer WH. J Chem Phys 1972;57:2843-54.

48. Yamakawa H, Shimada J. J Chem Phys 1985;83:2607-11.

49. Shimada J, Yamakawa H. J Chem Phys 1986;85:591-600.

50. Domb C, Barrett AJ. Polymer 1976;17:179-84.

51. Yamakawa H. Macromolecules 1992;25:1912-16.

52. Flory PJ. Principles of Polymer Chemistry. Ithaca, N. Y. : Cornell University Press, 1953.